# Integration of surface seismic, microseismic, and production logs for shale gas characterization: Methodology and field application

John Henry Alzate[1] and Deepak Devegowda[1]


## Abstract

Technologies such as horizontal drilling and multistage hydraulic fracturing are central to ensuring the viability of shale oil and gas resource development by maximizing contact with the most productive reservoir volumes. However, characterization efforts based on the use of well logs and cores, although very informative, may be associated with substantial uncertainty in interwell volumes. Consequently, this work is centered around the development of a predictive tool based on surface seismic data analysis to rapidly demarcate the most prolific reservoir volumes, to identify zones more amenable to hydraulic fracturing, and to provide a methodology to locate productive infill wells for further development. Specifically, we demonstrate that surface seismic attributes such as $\lambda\rho/\mu\rho$ crossplots can successfully be employed to quantitatively grade reservoir rocks in unconventional plays. We also investigate the role of seismically inverted Poisson's ratio as a fracability discriminator and Young's modulus as an indicator of total organic carbon richness and porosity. The proposed predictive tool for sweet spot identification relies on classifying reservoir volumes on the basis of their amenability to fracturing and reservoir quality. The classification scheme is applied to a field case study from the Lower Barnett Shale and we validate these results using production logs recorded in four horizontal wells and microseismic data acquired while fracturing these wells. The integration of seismic data, production logs, and microseismic data underscores the value of shale reservoir characterization with a diverse suite of measurements to determine optimal well locations and to locate hydraulic fracture treatments. A key advantage of the methodology developed here is the ease of regional-scale characterization that can easily be generalized to other shale plays.


## Introduction

In an attempt to reduce the United States' dependence on energy imports and to satisfy the ever-growing demand for energy, there has been an increasing emphasis on developing the vast hydrocarbon resources in unconventional accumulations of oil and gas, primarily in shale oil and shale gas plays. (Schenk and Pollastro, 2002; Bruner and Smosna, 2011). Because shales are characterized by extremely low permeabilities on the order of a few nanodarcies, development activity in these shales was somewhat limited until the early 2000s. With the rapid evolution and maturity of novel drilling and completion technologies over the past decade, shale plays now constitute a significant percentage of overall U.S. oil and gas production (EIA, 2011).

One of the key developments critical to making shale wells economically productive overextended periods of time is the use of hydraulic fracture treatments. In combination with horizontal well technology, shale gas wells are now orders of magnitude more productive than wells completed in similar settings in the 1990s to the early 2000s (Agrawal et al., 2012). Shale wells are now routinely completed with a suite of hydraulic fracture treatments in several stages (Bennett et al., 2006; Bruner and Smosna, 2011; EIA, 2011). The stages are designed to contact as much of the reservoir rock as possible, thereby creating highly conductive oil and gas migration pathways between the reservoir rock and the wellbore (Daniels et al., 2007; Cipolla et al., 2008; Mayerhofer et al., 2010; Zimmer, 2011; Cipolla et al., 2012; Yu and Aguilera, 2012).

Additionally, as our knowledge of shales has expanded from the classical homogeneous seal rock model to that of a reservoir rock characterized by considerable lateral and vertical variability, there is an increasing need to exploit this knowledge for optimal well and fracture placement. Recent laboratory experiments on cores (Kale, 2009), drill cuttings, log analysis, and seismic-derived images (Sullivan et al., 2006; Elebiju et al., 2010) emphasize the need for improved characterization of organic-rich shales because of the presence of short- and long-range heterogeneities that impact hydrocarbon storage, transport, and completion effectiveness (Cipolla et al., 2008, 2012). The work

[1]University of Oklahoma, Norman, Oklahoma, USA. E-mail: jhalzate@ou.edu; deepak.devegowda@ou.edu.

Manuscript received by the Editor 12 March 2013; published online 25 October 2013; corrected version published online 4 November 2013.This paper appears in *Interpretation*, Vol. 1, No. 2 (November 2013); p. SB37–SB49, 23 FIGS., 1 TABLE.

http://dx.doi.org/10.1190/INT-2013-0025.1. 

presented in this paper is organized around this main theme: to identify optimal locations for infill drilling and for hydraulic fracture treatments by mapping these heterogeneities and identifying the location and distribution of significant hydrocarbon accumulations to extract shale oil and gas resources more efficiently and economically.

Although the Barnett Shale is the most studied and well-known shale play in the USA (Boyer et al., 2006), several knowledge gaps related to integrating geologic, geophysical, petrophysical, and engineering data still exist (N. Gupta, personal communication, 2012). Studies by Kale (2009) and Gao (2011) are centered on petrophysical characterization and rock-typing based on cores and well log information. Singh (2008) instead relied on well logs to generate stratigraphic cross sections of the Barnett shale along with classification of the shale into 10 lithofacies, while Perez et al. (2011) generated templates for shales of varying compositions and porosities based on seismic-derived rock properties to enable targeting the most productive volumes of the reservoir which are also most conducive to hydraulic fracture stimulation.

To identify sweet spots in unconventional organic-rich shale reservoirs, it is generally recognized that the optimal placement of wells and hydraulic fracture treatments are controlled by reservoir quality, that is a function of porosity and total organic carbon (TOC) as well as completion effectiveness defined by the potential for fracture initiation and the ability for the fractures to remain open for extended periods of time (Cipolla et al., 2011). Cipolla et al. (2011) provide a comprehensive analysis of the factors affecting the reservoir quality and the completion effectiveness based on an analysis derived from the use of several field measurements such as sonic well logs, microseismic analysis, and seismic data. Maity and Amizadeh (2012) also present a similar approach for multiscale data integration for reservoir characterization using seismically inverted rock properties to extend well log data to interwell reservoir volumes to characterize shales. Refunjol et al. (2012), using a Barnett Shale case study, present a methodology to correlate hydraulic fracture-induced microseismic events with seismic attributes such as curvature and also explore the utility of $\lambda\rho/\mu\rho$ crossplots, but did not link the microseismic event distribution to rock brittleness.

Although these studies have expanded our understanding of shale reservoirs and the types of analyses necessary to quantify reservoir quality, the aforementioned workflows are somewhat limited because of the lack of validation with field production data. The work presented in this paper therefore is unique because, first, we derive a template based on seismic-derived attributes to quantify reservoir quality for regional and field-scale shale characterization. Second, we validate the template against production logs acquired in four horizontal wells completed with multiple-stage hydraulic fracture treatments. Reservoir performance monitoring, well completion evaluation, and planning and evaluation of well workovers are the most common applications of production logs (Riddle, 1962; McKinley, 1982; Hill, 1990). These production logs quantify gas production rates across each of the fracture stages and provide a means to validate the rock classification template. We then explore the relationship between the location of microseismic events and the $\lambda\rho/\mu\rho$ crossplots to characterize fracture propagation and profiles.

We also validate observations of brittleness in shales exhibiting low values of Poisson's ratios. Consequently, with the rock quality template generated from seismic-derived attributes of $\lambda\rho$ and $\mu\rho$, we are then able to provide reliable estimates of variations in rock quality laterally and vertically across shales, thereby enabling the successful placement of productive wells and hydraulic fracture treatments.

The paper is organized as follows: We first provide an overview of the petrophysical characteristics of the Barnett shale relevant to well performance and hydraulic fracture stimulation. We then describe a rock quality template based on seismic-derived attributes that extends the petrophysical characterization to regional- and field-scale volumes. Finally, we validate the rock quality template against production and microseismic data. The production data for each hydraulic fracture stage were acquired from production logs recorded four months following the start of production and represent the gas and water flow rates across each stage recorded at the time of the production log survey.

## Barnett Shale petrophysical characterization

Petrophysical characterization of a reservoir involves identifying rock types with similar flow and storage capacities (Kale et al., 2010a, 2010b). According to Gunter et al. (1997), a rock type is a unit of rock deposited under similar geologic conditions that underwent similar diagenetic processes resulting in unique porosity-permeability relationships, capillary pressure profile, and water saturations above free water.

Conventional methods of rock typing based on porosity-permeability crossplots do not work in shales due to the lack of dynamic range and the difficulties involved in the direct measurements of most of the petrophysical properties (Kale et al., 2010a, 2010b). Consequently, petrophysical characterization of shales has evolved to classification of petrotypes or rock types as a function of mineralogy, TOC, and shale mechanical properties. For example, Kale (2009) performed petrotyping based on core measurements acquired from three vertical wells located in the Newark East field within the core area of the Barnett. Kale (2009) performed several measurements over 1600 ft of core and identified three key measurements that control variability in the Barnett study area: porosity ($\varphi$), TOC, and total carbonate (TC). Gao (2011) analyzed the same data set using dimensionality reduction and

clustering algorithms to identify three petrotypes ranked as (1) good, (2) intermediate, or (3) poor, based on petrophysical properties and through correlation with production data in the cored wells. The general characteristics of petrotypes 1, 2, and 3 are provided in Figure 1. Hoeve et al. (2011) attempted to identify "sweet spots" through the use of well logs. Their basic premise was that the porosity thickness obtained from wireline logs is a fairly good indicator of reservoir quality. However, these efforts were restricted in their ability to predict hydraulic fracture efficacy because the mineralogical controls on fracture amenability were poorly understood at that time. Additionally, because these were restricted to core and well log data, the extension to interwell volumes was not so straightforward.

The work presented in this paper documents our approach to develop a reservoir rock quality classification template for locating infill wells and hydraulic fracture treatments successfully by integrating seismically inverted rock properties such as $\lambda\rho$, $\mu\rho$, Young's modulus, and Poisson's ratio with microseismic and production log data and describes a workflow to integrate multidisciplinary and multiscale subsurface data (3D seismic, production logs, and microseismic) to characterize twenty square miles in the Lower Barnett Shale play.

## Description of data acquired in the study area

Our work is based on a 3D seismic survey recorded in the Barnett core area in the Newark East field (Figure 2). The seismic data were inverted using a commercial inversion algorithm that requires angle-dependent wavelets and angle stacks and results in estimates of P-impedance, S-impedance, and density (Hampson and Rusell, 2005). The inversion results in the 3D seismic volume

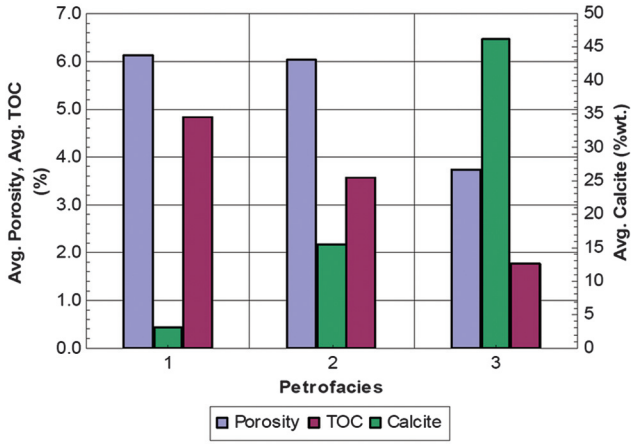


**Figure 1.** Average porosity, TOC, and average calcite content of the three petrotypes defined by Kale et al. (2010a, 2010b).

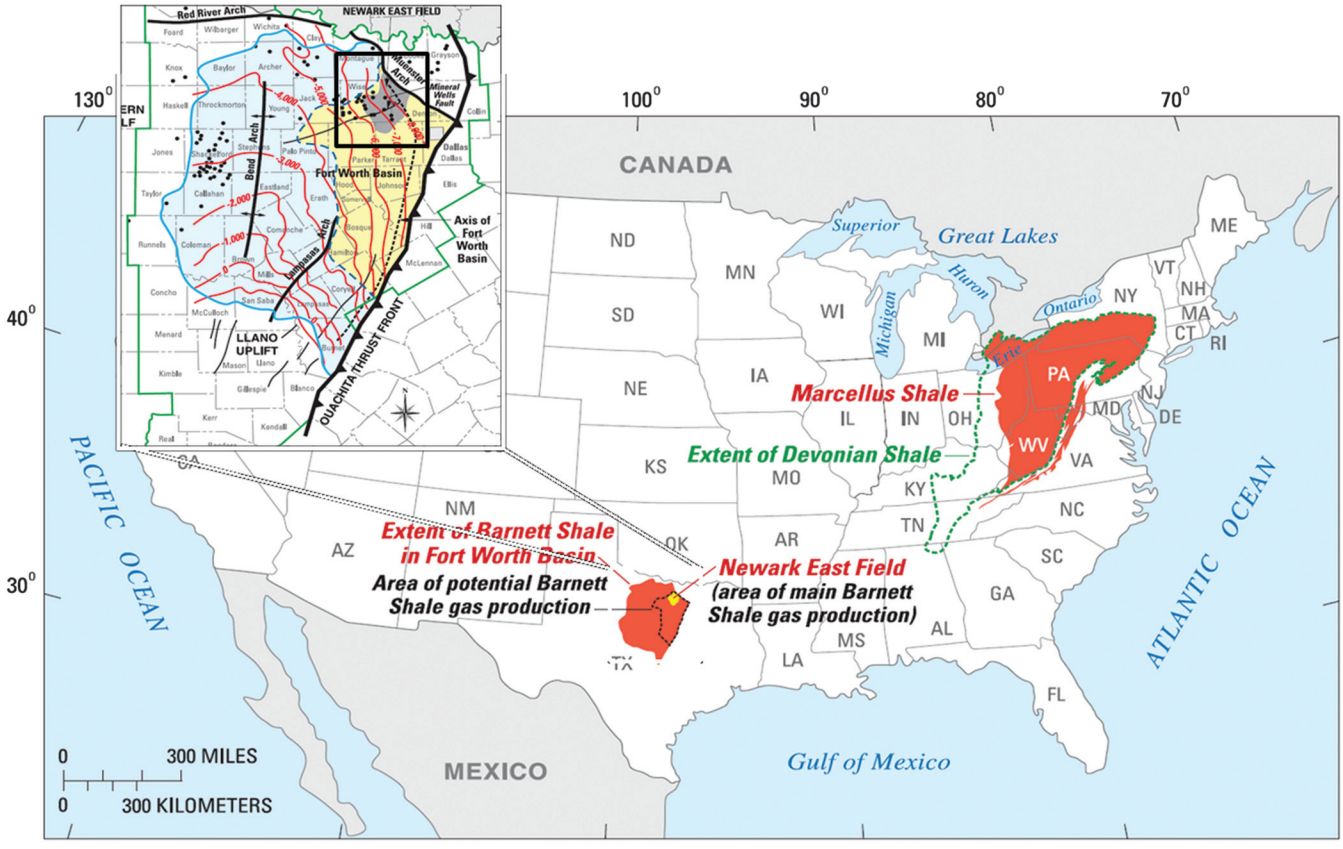


**Figure 2.** Location of Mississippian Barnett Shale, Fort Worth Basin. The top left square details a zoom in to the area of study. Modified from Bruner and Smosna (2011).

were calibrated to over 400 wells located in the survey area to ensure satisfactory reliability of the inversion results (Perez, 2013).

Once the P- and S-impedance volumes have been generated, they can be used to calculate the Lamé parameters of imcompressibility, $\lambda$, and rigidity, $\mu$. In conventional reservoirs, incompressibility has been shown to be more sensitive to the pore fluids than to the matrix and additionally, for elastic materials rigidity is only influenced by the matrix connectivity (Goodway et al., 1997, 1998; Smith, 1999; Dufor et al., 2002).

Even though the stimulation process was very similar across all four horizontal wells with similar number of fracturing stages, similar volumes of fluid and proppant pumped per stage, similar treatment times and pressures, the disparity in the production rates between the wells motivated the operator to acquire production logs to assess fracture effectiveness. The production logging suite for Wells A, B, C, and D comprised the temperature, pressure, deviation survey, and multispinner flowmeter logs. The multispinner flowmeter logs were chosen by the operator to enable scanning of the entire wellbore in horizontal laterals to properly quantify multiphase flow of gas and liquids. These were then analyzed for gas flow rates along the lateral, incremental gas and water production along the lateral, and gas and water hold up. These logs were recorded along the horizontal section where the wells were hydraulically fractured. Figures 3 and 4 show the incremental

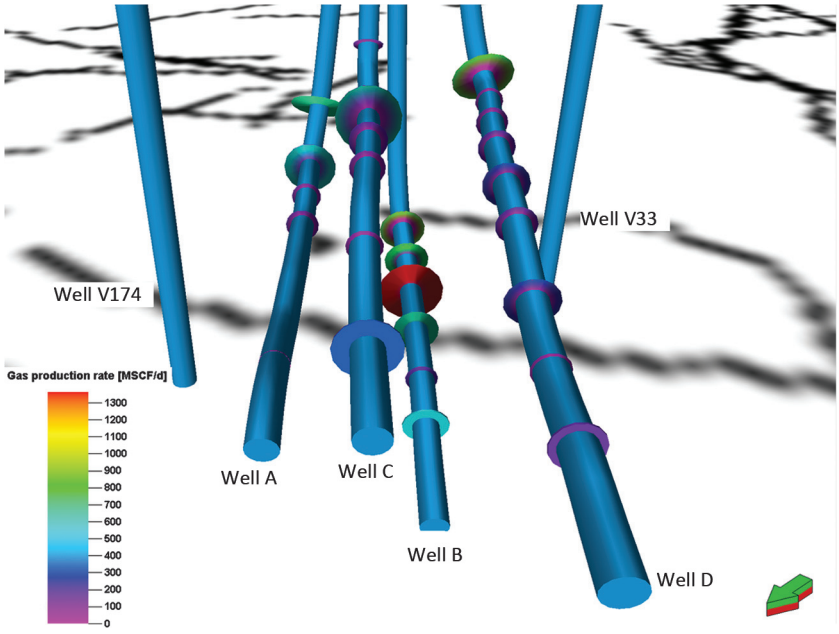


**Figure 3.** Differential gas production (MSCF/d) indicated by the color and diameter of the discs along the wellbores. The background is a depth slice matching the depth at which Well B is completed of a seismic attribute called *ant-tracked coherence*. Ant track is particularly well-suited to detect discontinuities in the subsurface.

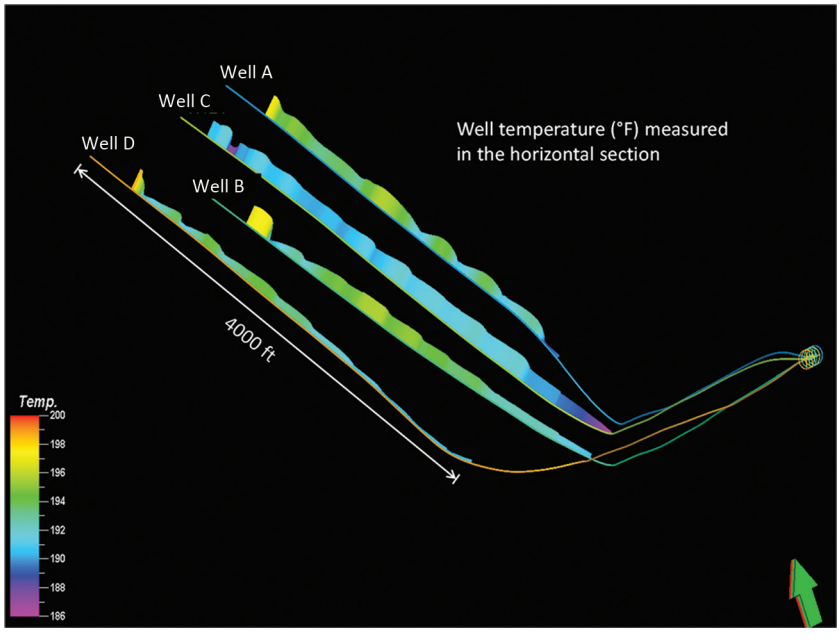


**Figure 4.** Top view of wells showing the temperature along the horizontal section of the four parallel horizontal wells drilled in the Lower Barnett Shale.

gas production log and the temperature log, respectively, for the four horizontal wells.

In Figure 3, the differential gas production, or gas production rate at each perforated interval, is indicated by the color of the disks along the wellbores. The diameters of the disks are scaled to the most productive stage in each well. The differential gas rate varies from a minimum of 80 MSCF/d to a maximum of 1250 MSCF/d and clearly demonstrates that, although the hydraulic fracture treatments were similar for all stages in all wells, there is a vast disparity in the production performance of each of the stages. The background is a seismic attribute called *ant-tracked coherence* which is particularly well-suited to demarcate faults and existing fractures at the time the seismic survey is recorded (Townsend et al., 1998; Jansen 2005; Chopra and Marfurt, 2008).

Figure 4 illustrates the flowing temperature logs recorded along each of the four horizontal well sections. Temperature logs are very useful to identify injection or production zones and are very sensitive to gas entry along the wellbore. Gas entry points typically correspond to a sharp temperature decrease and Figure 4 therefore demarcates locations of gas entry along the laterals. The cooling effect is due to the Joule-Thomson cooling as gas enters the wellbore from the formation through the casing perforations (Hill, 1990). The production rates recorded at each stage for each of the wells is provided in Table 1. Well B is the best-performing well, followed by Well D, Well C, and Well A.

## Methodology

In Perez et al. (2011), a workflow based on "heuristic" rock physics templates (Figure 5) was developed to guide the interpretation of seismically inverted properties in unconventional reservoirs. The shale reported in their study varies in composition from 60/40% quartz/clay to 100% quartz and porosity ranges from 0% to

**Table 1. Table showing the gas production rates per stage for each of the four production wells along with the classification of the rock volumes surrounding each fracture stage.**

| Well name | Gas rate per stage (MSCFD) | Well gas rate (MSCFD) | Rank | Reservoir quality | Gas rate per stage (MSCFD) |
|---|---|---|---|---|---|
| Well A | 650 | 1260 | 4 | Brittle-Poor | 650 |
| | 450 | | | Brittle-Poor | 450 |
| | 80 | | | Ductile-Poor | 80 |
| | 80 | | | Ductile-Poor | 80 |
| Well B | 650 | 4000 | 1 | Brittle-Rich | 650 |
| | 1250 | | | Brittle-Rich | 1250 |
| | 700 | | | Brittle-Rich | 700 |
| | 800 | | | Brittle-Rich | 800 |
| | 400 | | | Brittle-Rich | 400 |
| | 200 | | | Brittle-Rich | 200 |
| Well C | 250 | 1600 | 3 | Brittle-Poor | 250 |
| | 650 | | | Rich_Ductile | 650 |
| | 350 | | | Ductile-Poor | 350 |
| | 100 | | | Ductile-Poor | 100 |
| | 250 | | | Ductile-Poor | 250 |
| Well D | 850 | 2400 | 2 | Brittle-Poor | 850 |
| | 100 | | | Ductile-Poor | 100 |
| | 150 | | | Ductile-Poor | 150 |
| | 400 | | | Rich_Ductile | 400 |
| | 250 | | | Brittle-Poor | 250 |
| | 150 | | | Ductile-Poor | 150 |
| | 100 | | | Ductile-Poor | 100 |
| | 400 | | | Ductile-Poor | 400 |

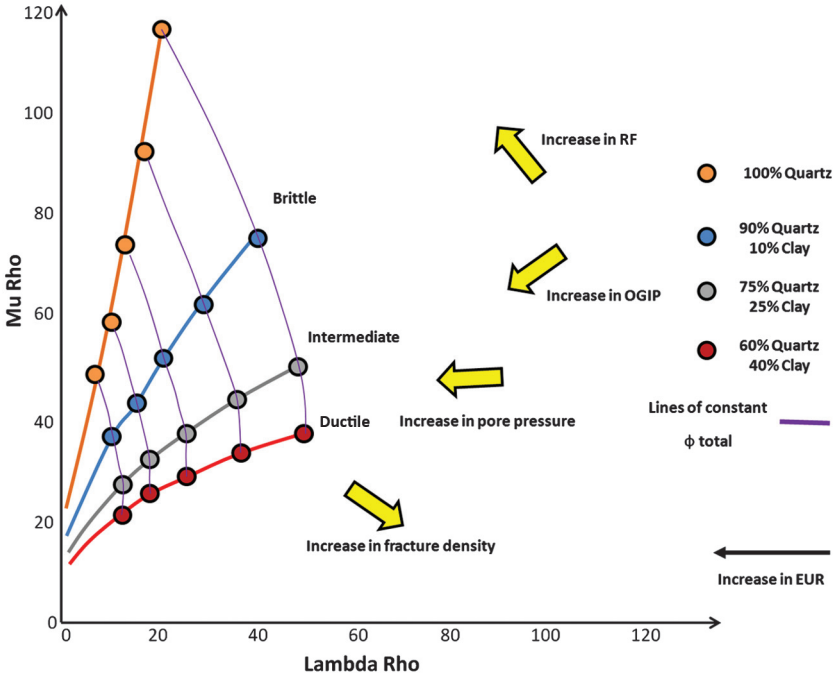


**Figure 5.** Heuristic template to interpret seismic, well log, or laboratory rock properties in terms of EUR, Original gas in place (OGIP), recovery factor (RF), pore pressure, and fracture density (Perez et al., 2011).

20%, but the underlying principles can easily be extended to interpretation in other shales with differing compositions. We provide a brief overview of their approach that we have adopted in this work.

Because the local gas-in-place estimates are linked to porosity, on the $\lambda\rho/\mu\rho$ crossplot (Figure 5), the gas-in-place or the richness of the rock is likely to track the porosity increase. Additionally, changes in rock composition are also directly related to the brittleness of the rock with quartz-rich rocks being brittle and clay-rich rocks ductile. In shales, the efficacy of the hydraulic fracture stimulation is linked to the extent of the stimulated reservoir volume and this is controlled by the brittleness of the rock. Moreover, brittle rocks can sustain propped fractures effectively while ductile rocks tend to heal themselves against the proppant. The recovery factor (RF) or fraction of hydrocarbons in place that can be produced is a function of these two properties: the richness of the rock, dictated by porosity, and the amenability to hydraulic fracturing, controlled by mineralogy and brittleness. Consequently, a rock quality template based on $\lambda\rho/\mu\rho$ crossplots is likely to be very informative for effective well and hydraulic fracture placement and forms the basis of this work.

The relationship between elastic properties such as the Young's modulus and reservoir quality properties such as porosity and TOC in shales has been well documented. Takahashi and Tanaka (2010) show that static as well as dynamic Young's modulus exhibit an inverse relationship to porosity in soft sedimentary rocks. Kumar et al. (2012) also document the inverse relationship between Young's modulus and porosity, TOC, and clay content based on nano-indentation tests on samples from the Woodford, Haynesville, Eagle Ford, and the Barnett Shale, finding similar trends for all plays. These studies demonstrate the usefulness of Young's modulus as an indicator of porosity and therefore gas-in-place and rock richness. Figure 6 shows the seismic-derived Young's modulus on a $\lambda\rho/\mu\rho$ crossplot and following the arguments provided by previous studies, the variation in the Young's modulus is a consequence of TOC and porosity differences.

The seismic data set was then analyzed to extract values of Poisson's ratios across the seismic volume and Figure 7 shows the corresponding values on a $\lambda\rho/\mu\rho$ crossplot. Figure 7 displays well-defined color bands representing portions of the data having similar Poisson's ratio and demarcates brittle zones that are associated with higher completion efficiency and that exhibit low values of Poisson's ratio. The higher values of Poisson's ratio associated with more ductile rocks are distinctly separated from the more brittle regions of this crossplot.

We then propose the following reservoir quality classification template as shown in Figure 8 obtained by combining Figures 6 and 7 that highlights Poisson's ratio and Young's modulus variations in the 3D seismic volume. These are: Group 0 or "Brittle and Rich" (red points) are those portions of the Barnett Shale having low values of Poisson's ratio and low values of Young's modulus; Group 1 or "Rich and Ductile" (yellow points) are those regions of the shale play characterized by high values of Poisson's ratio and low values of Young's modulus; in Group 2 or "Brittle and Poor" (green points) fall all portions of the shale play exhibiting low values of Poisson's ratio and high values of Young's modulus; and Group 3 or "Ductile and Poor" (blue points) are those parts of the shale play with high Poisson's ratio and high Young's modulus.

To create these plots, the seismic data were resampled into a geologic model discretized into $792 \times 540 \times 532$ ($xyz$) grid cells. Due to high the number of cells ($\sim 2.3 \times 10^8$), the number of operations and the amount of memory required to store the resampled data, the most suitable method to achieve resampling in the interpretation package is called *closest point*

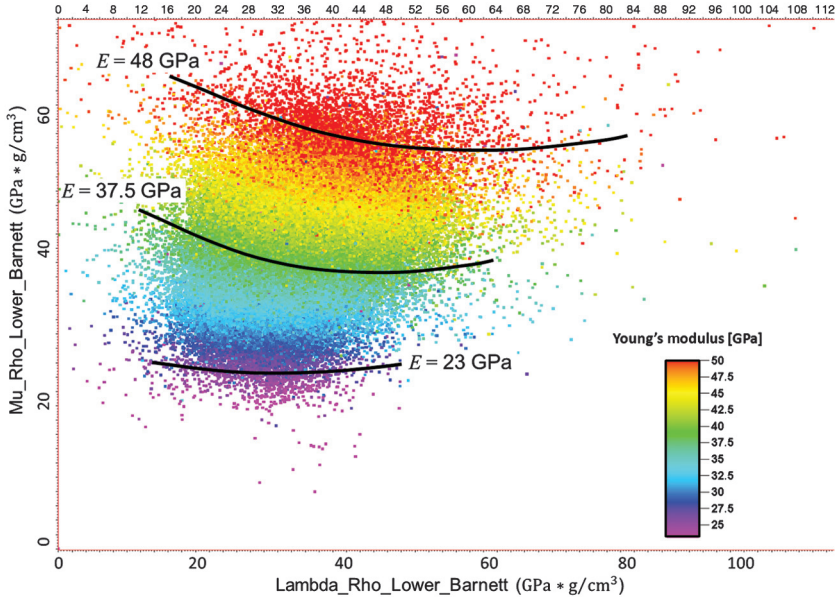


**Figure 6.** Seismic $\lambda\rho/\mu\rho$ crossplot for the Lower Barnett Shale. Color indicates the Young's modulus, E, decreasing toward the origin.

approach where each property cell has contributions only from the closest (or most central) seismic cell. Although this method is computationally efficient because it only considers the closest seismic cell, the resampled volume contains a small amount (less than 1%) of spurious data. Therefore, in Figure 8, there are a few points of Group 0 in the other three regions. A similar effect is observed for the other three groups.

## Results and analysis

To assess the validity of the classification scheme described above, we then explore the relationship between individual fracture stage gas production rates and the $\lambda\rho$ and $\mu\rho$ parameters in the immediate vicinity of each perforation cluster or fracture stage. The gas production rates for each stage along each of the four laterals were acquired from the production logs. In Figure 9, we overlay these gas production rates on the rock classification template previously defined.

The grouping of the most prolific and least productive fracture stages in Figure 9 clearly indicates a strong relationship between the fracture productivity and the properties of the rock surrounding the perforation clusters. The most prolific zones tend to be associated with the previously defined Group 0, while points located within Group 3 are relatively less productive. Consequently, Figure 9 provides strong evidence that supports the motivating factors for this work: (1) that the productivity of shale well fractures is determined

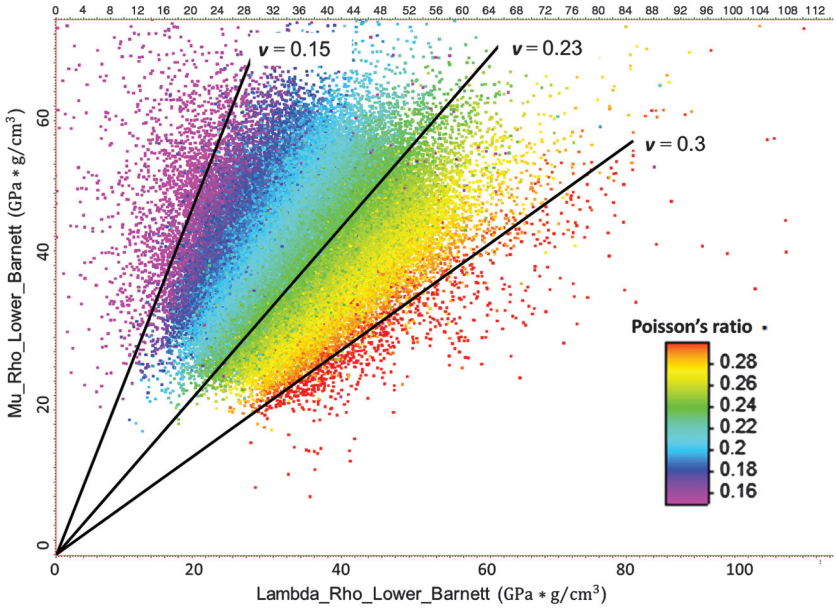


**Figure 7.** $\lambda\rho/\mu\rho$ crossplot for the Lower Barnett Shale. Color indicates the Poisson's ratio versus lines of fixed Poisson's ratio converge at the origin.

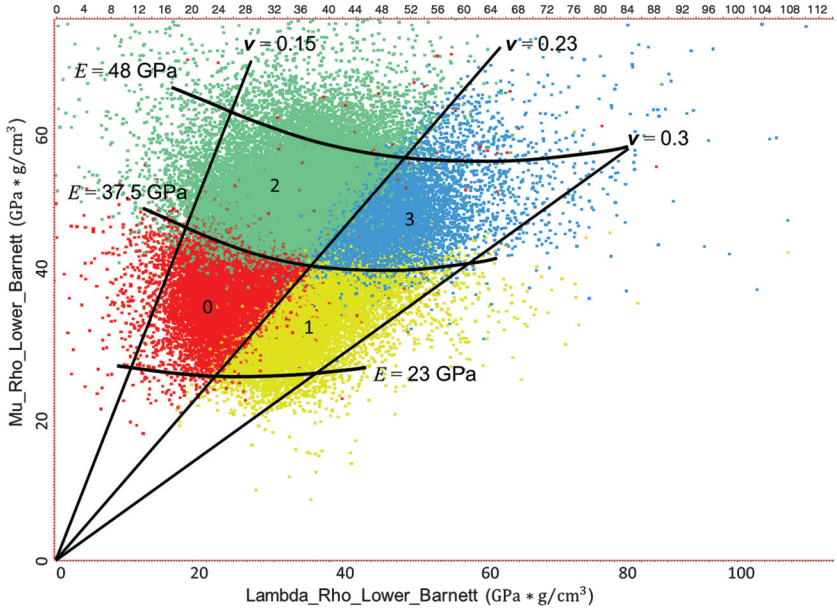


**Figure 8.** Lower Barnett reservoir quality classification based on seismically inverted rock properties. Four groups are defined: Group 0 or "Brittle and Rich," Group 1 or "Rich and Ductile," Group 2 or "Brittle and Poor," and Group 3 or "Ductile and Poor."

by the mechanical properties and richness of the rock in the vicinity of the completion and (2) that seismic-derived properties enable classification of rock types on a regional scale.

In Figure 10, we modify the plot in Figure 7 illustrating Poisson's ratios in the regions surrounding each of the four horizontal laterals and demarcate with ovals the values corresponding to the perforated zones in Well A, Well B, Well C, and Well D. The strong correlation between the Poisson's ratio and the well production rate is underscored by the location of the most productive Well B whose $\lambda\rho/\mu\rho$ points fall in the region associated with smallest Poisson's ratios. For the other wells, a progressive decrease in well performance is strongly related to the corresponding values of the Poisson's ratios adjacent to the wellbore. Figures 11–14 examine the performance of each fracture stage on a well-by-well basis with the same conclusions.

Because we now have a rock classification template, we can also analyze the distribution of the rock types in relation to the location of the horizontal laterals of each of the wells. Figure 15 shows a vertical slice across a 390-ft section of the lower Barnett and the corresponding well locations. The figure reinforces our earlier observations supporting the substantially higher productivity of Well B, completed in the brittle-rich zone, in comparison to the other wells completed in less attractive target layers. Additionally, we also analyzed the spatial variations of the distribution of these rock types in four stratal slices in Figures 16–19 for each of the four wells. The detailed map view of these figures confirms the observations made earlier in Figure 15 regarding the link between well performance and the distribution of the most productive rock types.

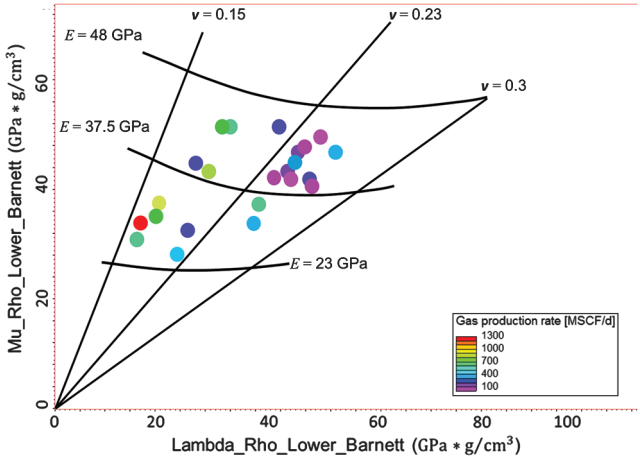


**Figure 9.** Seismic $\lambda\rho/\mu\rho$ extracted along the wellbores with production logs. The color indicates the gas rate at each individual perforation.

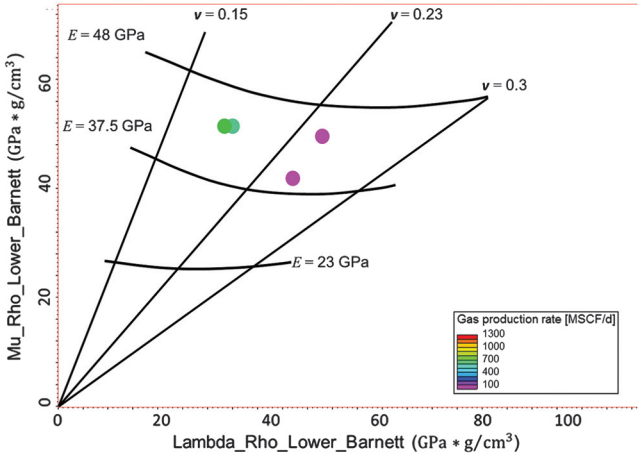


**Figure 11.** Seismic $\lambda\rho/\mu\rho$ extracted along the wellbores with production logs. The color indicates the gas rate at each individual perforation in Well A.

**Figure 10.** $\lambda\rho/\mu\rho$ crossplot for the Lower Barnett Shale. Color indicates the Poisson's ratio. Ovals indicate the range of values observed in the producing zones for each well.

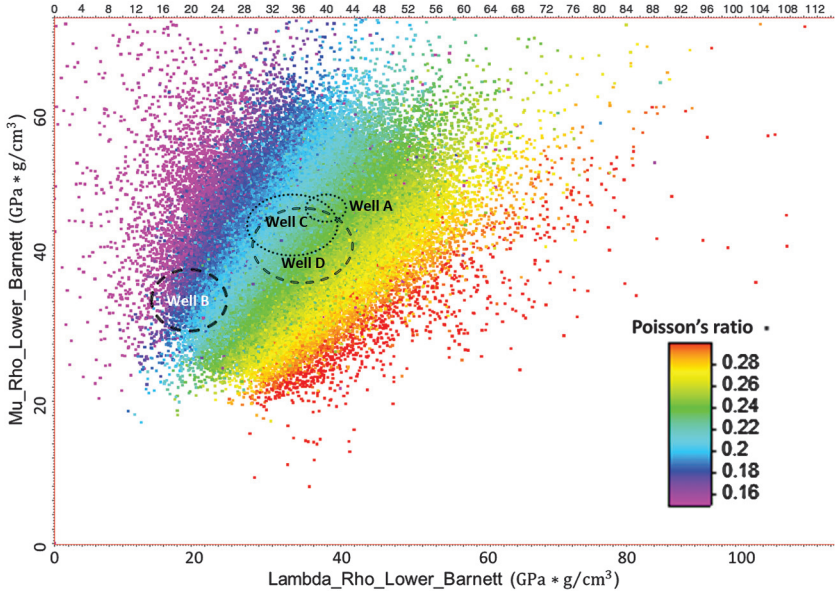

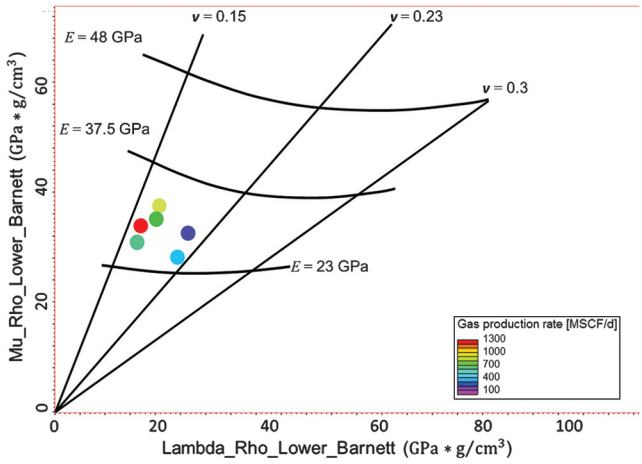


**Figure 12.** Seismic $\lambda\rho/\mu\rho$ extracted along the wellbores with production logs. The color indicates the gas rate at each individual stage in Well B.

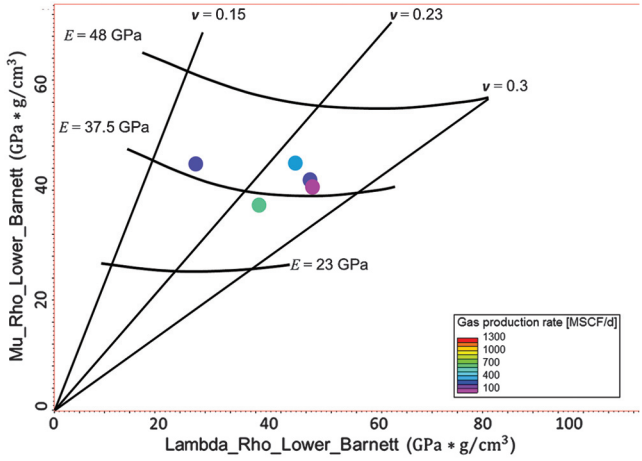


**Figure 13.** Seismic $\lambda\rho/\mu\rho$ extracted along the wellbores with production logs. The color indicates the gas rate at each individual stage in Well C.

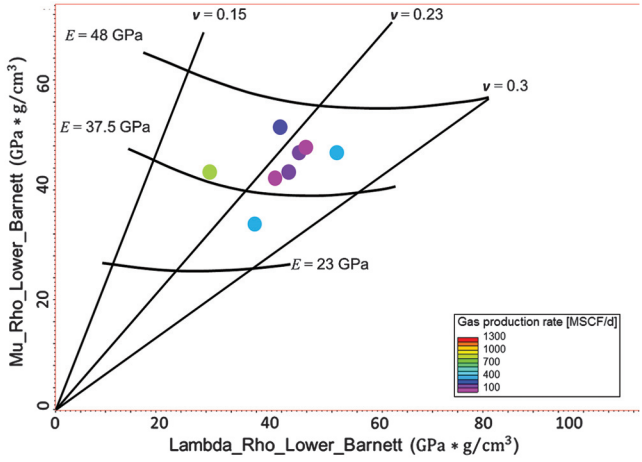


**Figure 14.** Seismic $\lambda\rho/\mu\rho$ extracted along the wellbores with production logs. The color indicates the gas rate at each individual stage in Well D.

We then also employed the microseismic data recorded while fracturing these wells to map the stimulated volume of rock. Our goal was to analyze the patterns of fracture growth and their relation to the rock classification template described earlier. In Figures 20–23, we plot the $\lambda\rho/\mu\rho$ values corresponding to the microseismic events measured for Wells A, B, C, and D, respectively. Additionally, in these figures, we also indicate by means of a histogram the percentage of all recorded events located within the different rock classes. An interesting observation is that, irrespective of the location of the lateral, fracture events are preferentially clustered in the brittle rock types with roughly

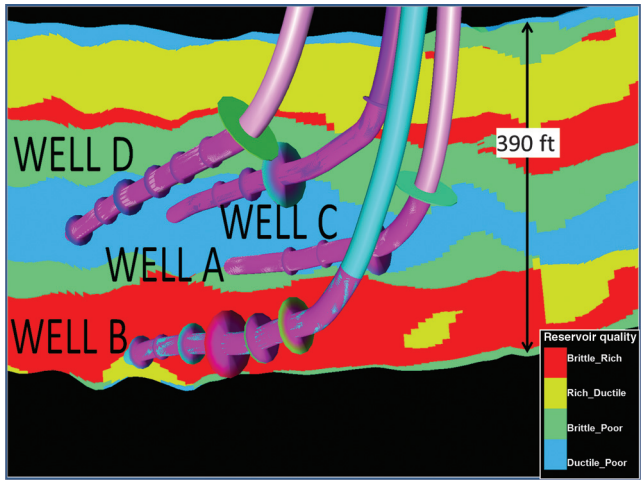


**Figure 15.** East–west vertical slice through the reservoir quality volume showing the location of the wells having production logs. The color in the layers is following the rock classification proposed. Well B is entirely completed in a Brittle-Rich (red) layer, while most of Well A, Well C, and Well D rest in a Ductile-Poor (blue) layer.

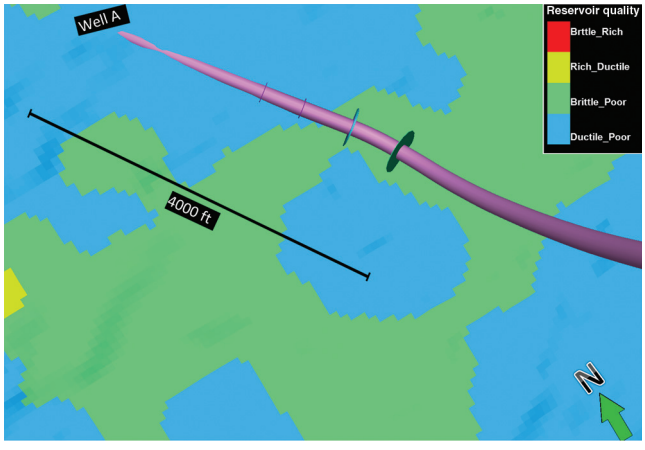


**Figure 16.** Map view of the stratal slice through the reservoir quality volume at the level where Well A is completed. The colors represent the rock quality distribution according to the rock classification proposed.

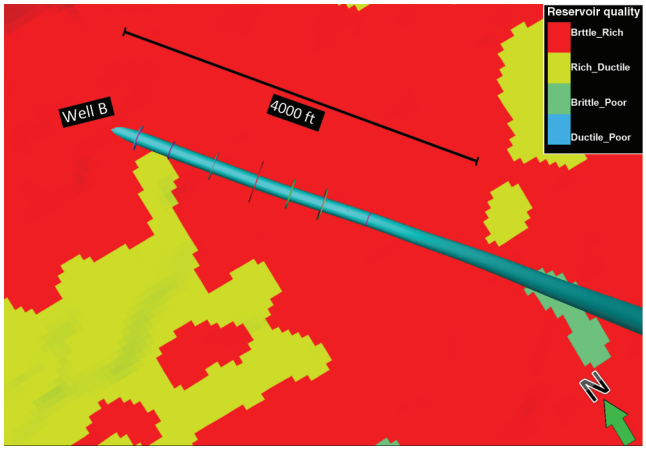


**Figure 17.** Map view of the stratal slice through the reservoir quality volume at the level where Well B is completed. The colors represent the rock quality distribution according to the rock classification proposed.

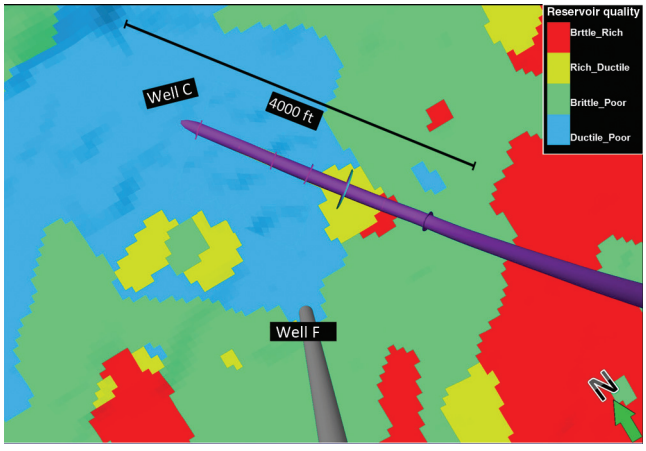


**Figure 18.** Map view of the stratal slice through the reservoir quality volume at the level where Well C is completed. The colors represent the rock quality distribution according to the rock classification proposed.

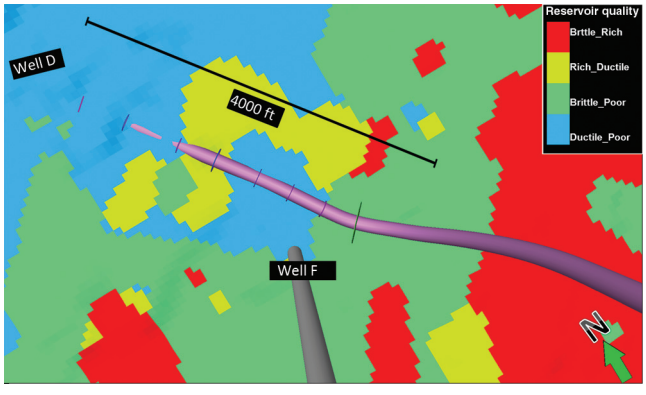


**Figure 19.** Map view of the stratal slice through the reservoir quality volume at the level where Well D is completed. The colors represent the rock quality distribution according to the rock classification proposed.

65%–70% of all events for all wells are recorded in the brittle red and green clusters.

To summarize, we provide the flow rates and rock classes associated with each stage of each well in Table 1. The data also provides the total production per well and a well ranking based on these numbers. The rock classes recorded in Column 5 of Table 1 show excellent correlation with the individual fracture stage productivity with high accuracy, although there are a few stages, one each in Wells B, C, and D that do not conform to this classification. However, in general, the classification correlates with productivity very satisfactorily and Well B, the most productive well, is entirely completed in a Brittle and Rich zone. For the

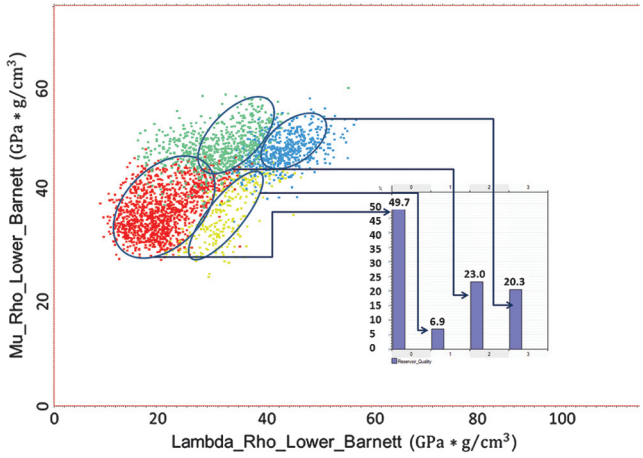


**Figure 20.** $\lambda\rho/\mu\rho$ crossplots showing the microseismic events recorded while hydraulically fracturing Well A. About 73% of the microseismic events recorded while stimulating Well A fall in portions of the rock classified as Brittle according to this reservoir quality classification.

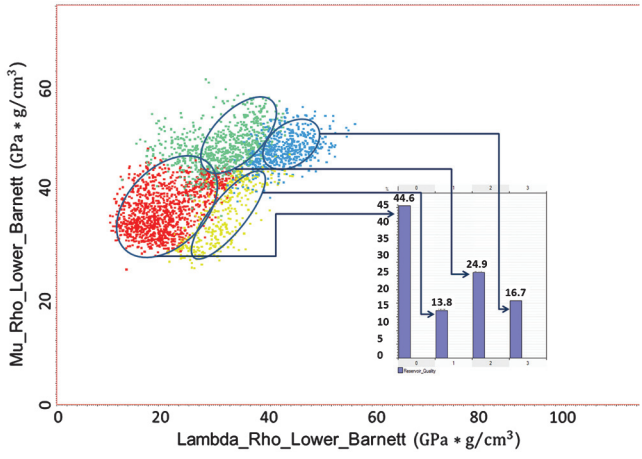


**Figure 21.** $\lambda\rho/\mu\rho$ crossplots showing the microseismic events recorded while hydraulically fracturing Well B. About 70% of the MS events recorded while stimulating Well B fall in portions of the rock classified as Brittle according to this reservoir quality classification.

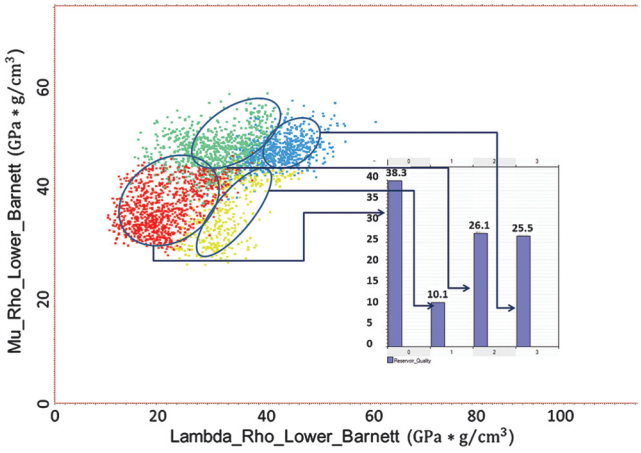


**Figure 22.** $\lambda\rho/\mu\rho$ crossplots showing the microseismic events recorded while hydraulically fracturing Well C. About 64% of the MS events recorded while stimulating Well C fall in portions of the rock classified as Brittle according to this reservoir quality classification.

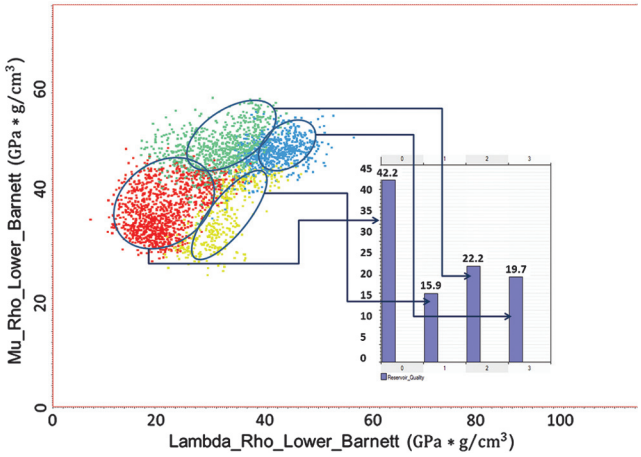


**Figure 23.** $\lambda\rho/\mu\rho$ crossplots showing the microseismic events recorded while hydraulically fracturing Well D. About 65% of the microseismic events recorded while stimulating Well D fall in portions of the rock classified as Brittle according to this reservoir quality classification.

other three wells, the perforations completed in zones with good fracability (green) are distinct from most of the other stages completed in Poor and Ductile regions (blue) in terms of productivity.

## Conclusions

The work presented in this paper demonstrates a promising approach to use 3D surface seismic data, microseismic, and production logs for regional-scale reservoir characterization. The 3D seismic data set was inverted for attributes such as the $\lambda\rho/\mu\rho$ parameters which were then used to classify reservoir sweet spots on the basis of rock properties such as the Young's Moduli and Poisson's ratios. The proposed classification template was validated against a data set acquired in the Lower Barnett shale play where we demonstrate the link between reservoir quality and amenability to hydraulic fracturing in four horizontal wells with multiple stage completions.

Although the proposed template was successfully applied to a field-case study, the extension of this approach to other shale plays is likely to require careful consideration of the relationships between rock mechanical properties, seismic attributes and petrophysical properties such as porosity, TOC, and mineralogy.

## Acknowledgments

The authors especially want to thank the people at DEVON Energy for releasing this unique data set that led to an exciting research study. We also want to thank Roderick Perez of the University of Oklahoma for doing the time-depth conversion and the seismic inversion and Kurt J. Marfurt for his valuable feedback.

## References

Agrawal, A., Y. Wei, and S. A. Holditch, 2012, A technical and economic study of completion techniques in five emerging US gas shales: A Woodford Shale example: SPE, **27**, 39–49, SPE 135396, doi: 10.2118/135396-PA.

Bennett, L., J. LeCalvez, D. R. Sarver, K. Tanner, W. S. Birk, G. Waters, J. Drew, G. Michaud, P. Primiero, L. Eisner, R. Jones, D. Leslie, M. J. Williams, J. Govenlock, R. C. Klem, and K. Tezuka, 2006, The source for hydraulic fracture characterization: Oilfield review/Schlumberger, 42–57.

Boyer, C., J. Kieschnick, R. Suarez-Rivera, R. E. Lewis, and G. Waters, 2006, Producing gas from its source: Oilfield review/Schlumberger, 36–49.

Bruner, K. R., and R. Smosna, 2011, A comparative study of the Mississippian Barnett Shale, Fort Worth Basin, and Devonian Marcellus Shale, Appalachian Basin: Technical Report DOE/NETL-2011/1478, National Energy Technology Laboratory (NETL) for The United States Department of Energy.

Chopra, S., and K. J. Marfurt, eds., 2008, Seismic attributes for prospect identification and reservoir characterization,: SEG, 208–210.

Cipolla, C., R. Lewis, S. Maxwell, and M. Mack, 2011a, Appraising unconventional resource plays: Separating reservoir quality from completion effectiveness: International Petroleum Technology Conference, Paper IPTC 14677.

Cipolla, C., S. Maxwell, and M. Mack, 2012, Engineering guide to the application of microseismic interpretations: Hydraulic Fracturing Conference, SPE, Paper SPE 152165, doi: 10.2118/152165-MS.

Cipolla, C., N. R. Warpinski, M.J. Mayerhofer, E. P. Lolon, and M. C. Vincent, 2008, The relationship between fracture complexity, reservoir properties, and fracture treatment design: Annual Technical Conference and Exhibition, SPE, Paper SPE 115769.

Daniels, J., G. Waters, J. LeCalvez, J. Lassek, and D. Bentley, 2007, Contacting more of the Barnett Shale through an integration of real-time microseismic monitoring, petrophysics and hydraulic fracture design: Annual Technical Conference and Exhibition, SPE, Paper SPE 110562.

Dufor, J., J. Squires, W. N. Goodway, A. Edmunds, and I. Shook, 2002, Integrated geological and geophysical interpretation case study and Lame rock parameter extractions using AVO analysis on the Blacfoot 3C-3D seismic data, South Alberta, Canada: Geophysics, **67**, 27–37, doi: 10.1190/1.1451319.

Elebiju, O. O., G. R. Keller, and K. J. Marfurt, 2010, Investigation of links between Precambrian basement structure and Paleozoic strata in the Fort Worth Basin, Texas, U.S.A., using high-resolution aeromagnetic (HRAM) data and seismic attributes: Geophysics, **75**, no. 4, B157–B168, doi: 10.1190/1.3435939.

Energy Information Administration (EIA), 2011. Natural gas production.

Gao, C., 2011, Multiscale ensemble Kalman filter for history matching and characterization of Barnett Shale: M.S. thesis, University of Oklahoma.

Goodway, B., T. Chen, and J. Downton, 1997, Improved AVO fluid detection and lithology discrimination using Lame petrophysical parameters; "$\lambda\rho$', "$\mu\rho$", & "$\lambda/\mu$" fluid stack, from P and S inversions: 67th Annual International Meeting, SEG, Expanded Abstracts, 183–186.

Goodway, W., T. Chen, and J. Downton, 1998, Joint P-P and P-S inversion of a walkaway VSP for Vp, Vs, and Vp/VS compared to log data and for surface P-P calibration and inversion: SEG Post-Convention Workshop "Can P-wave AVO be quantitative or do we need multicomponent."

Gunter, G. W., J. M. Finneran, D. J. Hartmann, and J. D. Miller, 1997, Early determination of reservoir flow units using an integrated petrophysical method: Annual Technical Conference and Exhibition, SPE, Paper SPE 38679.

Hampson, D. P., and T. E. Rusell, 2005, Simultaneous inversion of pre-stack seismic data: 75th Annual International Meeting, SEG, Expanded Abstracts, 1633–1637.

Hill, D. H., 1990, Production logging-theoretical and interpretive elements: Monograph Series, SPE, **14**, 145.

Hoeve, M. V., S.C. Meyer, J. Preusser, and A. Makowitz, 2011, Basin-wide delineation of gas shale "sweet spots" using density and neutron logs; implications for qualitative and quantitative assessment of gas shale resources: Hedberg Conference, AAPG.

Jansen, K., 2005, Seismic investigation of wrench faulting and fracturing at Rulison Field, Colorado: M.S. thesis, Colorado School of Mines, 34–59.

Kale, S., 2009, Petrophysical characterization of Barnett Shale play: M.S. thesis, University of Oklahoma.

Kale, S., C. S. Rai, and C. H. Sondergeld, 2010a, Petrophysical characterization of Barnett Shale: Unconventional Gas Conference, SPE, Paper SPE 131770.

Kale, S., C. S. Rai, and C. H. Sondergeld, 2010b, Rock typing in gas shales: Annual Technical Conference and Exhibition, SPE, Paper SPE 134539.

Kumar, V., C. H. Sondergeld, and C. S. Rai, 2012, Nano to macro mechanical characterization of shale: Annual Technical Conference and Exhibition, SPE, Paper SPE 159808-PP.

Maity, D., and F. Aminzadeh, 2012, Reservoir characterization of an unconventional reservoir by integrating microseismic, seismic, and well log data: SPE Western Regional Meeting, Paper SPE 154339.

Mayerhofer, M. J., E. P. Lolon, N. R. Warpinski, C. L. Cipolla, D. Waiser, and C. M. Rightmire, 2010, What is stimulated reservoir volume?: SPE Production and Operations, 89–98.

McKinley, R. M., 1982, Production logging: International Petroleum Exhibition and Technical Symposium, SPE, Paper SPE 10035.

Perez, M., D. Close, B. Goodway, and G. Purdue, 2011, Developing templates for integrating quantitative geophysics and hydraulic fracture completions data: Part I — Principles and theory: 81st Annual International Meeting, SEG, Expanded Abstracts, 1794–1798.

Perez, R., 2013, Correlation of surface seismic measurements to completion quality: Application to the Barnett Shale: Ph.D. dissertation, University of Oklahoma.

Refunjol, X. E., K. M. Keranen, J. H. LeCalvez, and K. J. Marfurt, 2012, Integration of hydraulically induced microseismic events location with active seismic attributes: A North Texas Barnett Shale case study: Geophysics, **77**, no. 3, KS1–KS12, doi: 10.1190/geo2011.0032.1.

Riddle, G. A., 1962, Acoustic wave propagation in bonded and unbonded oil well casing: Annual Technical Conference and Exhibition, SPE, Paper SPE 454.

Schenk, C. J., and R. M. Pollastro, 2002, Natural gas production in the United States: National Assessment of Oil and Gas Series: USGS Fact Sheet FS-113-01.

Singh, P., 2008, Lithofacies and sequence stratigraphic framework of the Barnett Shale, Northeast Texas: Ph.D. dissertation, The University of Oklahoma.

Smith, G. C., 1999, The relationship between Lamé's constants, Lambda and Mu, and the fluid factor in AVO analysis of seismic data: South African Geophysical Association Meeting, Abstracts 6.3.

Sullivan, E. C., K. J. Marfurt, A. Lacazette, and M. Ammerman, 2006, Application of new seismic attributes to collapse chimneys in the Fort Worth Basin: Geophysics, **71**, no. 4, B11–B119, doi: 10.1190/1.2216189.

Takahashi, T., and S. Tanaka, 2010, Rock physics model for interpreting dynamic and static Young's moduli of soft sedimentary rocks: Presented at the IRSM International Symposium and 6th Asian Mechanics Symposium on Advances in Rock Engineering.

Townsend, C., I. R. Firth, and R. Westerman, 1998, Small seismic-scale fault identification and mapping, *in* G. Jones, Q. J. Fisher, and R. J. Knipe, eds., Faulting, fault

sealing and fluid flow in hydrocarbon reservoirs: Geological Society London Special Publications, **147**, 1–25.
Yu, G., and R. Aguilera, 2012, 3D analytical modeling of hydraulic fracturing stimulated reservoir volume: Latin American and Caribbean Petroleum Engineering Conference, SPE, Paper SPE 153486.
Zimmer, U., 2011, Calculating stimulated reservoir volume (SRV) with consideration of uncertainties in microseismic-event locations: Canadian Unconventional Resources Conference, Paper CSUG/SPE 145610.

Biographies and photographs of authors are not available.